




OPEN

Synthesis, molecular docking, and in vivo antidiabetic evaluation of new benzylidene-2,4-thiazolidinediones as partial PPAR- γ agonists

Asim Najmi¹, Md Shamsher Alam¹, Neelaveni Thangavel¹, Manal M. E. Taha², Abdulkarim M. Meraya³, Mohammed Albratty¹, Hassan A. Alhazmi^{1,2,4}, Waqar Ahsan¹, Anzarul Haque⁵ & Faizul Azam⁶

Peroxisome proliferator-activated receptor- γ (PPAR- γ) partial agonists or antagonists, also termed as selective PPAR- γ modulators, are more beneficial than full agonists because they can avoid the adverse effects associated with PPAR- γ full agonists, such as weight gain and congestive heart disorders, while retaining the antidiabetic efficiency. In this study, we designed and synthesized new benzylidene-thiazolidine-2,4-diones while keeping the acidic thiazolidinedione (TZD) ring at the center, which is in contrast with the typical pharmacophore of PPAR- γ agonists. Five compounds (5a–e) were designed and synthesized in moderate to good yields and were characterized using spectral techniques. The in vivo antidiabetic efficacy of the synthesized compounds was assessed on streptozotocin-induced diabetic mice using standard protocols, and their effect on weight gain was also studied. Molecular docking and molecular dynamics (MD) simulation studies were performed to investigate the binding interactions of the title compounds with the PPAR- γ receptor and to establish their binding mechanism. Antidiabetic activity results revealed that compounds 5d and 5e possess promising antidiabetic activity comparable with the standard drug rosiglitazone. No compound showed considerable effect on the body weight of animals after 21 days of administration, and the findings showed statistical difference ($p < 0.05$ to $p < 0.0001$) among the diabetic control and standard drug rosiglitazone groups. In molecular docking study, compounds 5c and 5d exhibited higher binding energies (-10.1 and -10.0 kcal/mol, respectively) than the native ligand, non-thiazolidinedione PPAR- γ partial agonist (nTZDpa) (-9.8 kcal/mol). MD simulation further authenticated the stability of compound 5c-PPAR- γ complex over the 150 ns duration. The RMSD, RMSF, rGyr, SASA, and binding interactions of compound 5c-PPAR- γ complex were comparable to those of native ligand nTZDpa-PPAR- γ complex, suggesting that the title compounds have the potential to be developed as partial PPAR- γ agonists.

Abbreviations

Ala	Alanine
ANOVA	Analysis of variance
Arg	Arginine
BGL	Blood glucose levels
Cys	Cysteine

¹Department of Pharmaceutical Chemistry, College of Pharmacy, Jazan University, P. Box No. 114, Jazan, Saudi Arabia. ²Substance Abuse and Toxicology Research Centre, Jazan University, P. Box No. 114, Jazan, Saudi Arabia. ³Pharmacy Practice Research Unit, Department of Clinical Pharmacy, College of Pharmacy, Jazan University, Jazan, Saudi Arabia. ⁴Medical Research Center, Jazan University, Jazan, Saudi Arabia. ⁵Department of Pharmaceutics, Buraydah College of Dentistry and Pharmacy, P.O. Box 31717, Buraydah, Al-Qassim, Saudi Arabia. ⁶Department of Pharmaceutical Chemistry and Pharmacognosy, Unaizah College of Pharmacy, Qassim University, Unaizah, Saudi Arabia. ✉email: anajmi@jazanu.edu.sa

DM	Diabetes mellitus
DMSO	Dimethyl sulfoxide
FBG	Fasting blood glucose
FT-IR	Fourier transform-infrared spectrometry
Gly	Glycine
Glu	Glutamic acid
His	Histidine
ICH	International Conference on Harmonization
Ile	Isoleucine
LD ₅₀	Median lethal dose
Leu	Leucine
MD	Molecular dynamics
Met	Methionine
NMR	Nuclear magnetic resonance
nTZDpa	Non-thiazolidinedione PPAR- γ partial agonist
OECD	Organization for Economic Cooperation and Development
OGT	Oral glucose tolerance test
<i>p</i>	Level of significance
PDB	Protein data bank
Phe	Phenylalanine
PPAR- γ	Peroxisome proliferator-activated receptor- γ
rGyr	Radius of gyration
RCSB	Research Collaboratory for Structural Bioinformatics
RESPA	Reversible reference system propagator algorithm
RMSD	Root-mean-square deviation
RMSF	Root-mean-square fluctuation
SEM	Standard error of the mean
Ser	Serine
SASA	Solvent-accessible surface area
SPPARM	Selective PPAR- γ modulators
STZ	Streptozotocin
TG	Triglyceride
Thr	Threonine
TLC	Thin-layer chromatography
TZD	Thiazolidinediones

One of the major growing threats for the human population worldwide is diabetes mellitus (DM), and a considerable percentage of human population is currently suffering from type 1 or 2 DM¹. Although several antidiabetic drugs of different classes are available in the market, most of them are associated with minor to serious side effects^{2,3}. One of the drug classes used for type 2 DM is thiazolidinediones (TZDs) or glitazones, which act as insulin sensitizers. They regulate the transcription of genes responsible for glucose and lipid metabolism via binding to the peroxisome proliferator-activated receptor- γ (PPAR- γ)⁴. Through PPAR- γ stimulation, glitazones also regulate cell development, angiogenesis, and inflammation, which broadens their restorative potential⁴.

The positive correlation between adipogenesis and PPAR- γ action signifies the undesirable weight gain linked to the use of TZDs in people with DM and obesity^{5,6}. TZDs have also been reported to have other serious adverse effects, such as cardiotoxicity, congestive heart failure, and even conceivable carcinogenesis in a few cases^{7,8}. Hence, the pleiotropic effects of TZDs must be clarified to ensure medication safety and facilitate novel drug design and development. Selective PPAR- γ modulators (SPPARMs), also known as the partial agonists/antagonists of PPAR- γ subtype, disengage insulin sensitization from triglyceride (TG) accumulation in people with type 2 DM⁹. SPPARMs also help avoid the unfavorable effects of using full agonists, such as body weight gain and cardiotoxicity.

Several new derivatives with or without the TZD ring system have been designed and tested for their partial agonistic activities on PPAR- γ , resulting in the identification of various pharmacophores that could bind partially at the binding site of the protein^{10,11}. In this study, we designed new benzylidene-2,4-thiazolidinediones by keeping the acidic polar head in between the lipophilic ring and the linker instead of placing it at the end, which is typical for full agonists. This new strategy was expected to have effect on the binding to the receptor, which was studied using molecular docking by investigating the plausible interactions between the molecule and protein. The antidiabetic potential of the newly synthesized derivatives was assessed using an in vivo antidiabetic rodent model.

Materials and methods

Chemicals, reagents, and instruments

All the chemicals, reagents, and solvents used in this study were purchased from Sigma Aldrich (Steinheim, Germany) and used without further purification. The melting points of all synthesized compounds were measured by the open capillary method using a melting point apparatus (Stuart SMP30, Massachusetts, USA). The infrared (IR) spectra of the compounds were recorded using a Fourier transform-infrared spectrometer (FT-IR) coupled with attenuated total reflectance (FTIR-ATR) (Nicolet iS10, Thermo Scientific, Massachusetts, USA). The nuclear magnetic resonance (NMR) spectra of the synthesized compounds were obtained using NMR

spectrometer (Bruker 500 Ultra shield, Massachusetts, USA) operating at 500 MHz frequency for ^1H NMR and 100 MHz frequency for ^{13}C NMR analysis using dimethyl sulfoxide (DMSO) as the solvent and tetramethylsilane as the internal standard. The mass spectra (MS) were recorded using a triple quadrupole mass spectrometer (ThermoFisher Scientific, Massachusetts, USA). The completion of reactions was monitored using thin-layer chromatography (TLC) on precoated (F-254) aluminum-supported TLC plates (Merck, Darmstadt, Germany). Benzene: methanol (9:1) was used as the solvent system, and the retardation factor (R_f) was calculated.

Animals

In vivo studies were performed on male Swiss albino mice obtained from the central animal house facility, Jazan University, Saudi Arabia and were kept in the animal house at the College of Pharmacy until experiments were performed. All the animals were acclimatized for 1 week under standard conditions with a temperature of 22 ± 1 °C and humidity of $50\% \pm 5\%$ with a 12 h light/dark cycle and had free access to commercial food pellets and fresh tap water. The experimental protocol was approved by the Standing Committee for Scientific Research Ethics-Jazan University (HAPO-10-Z-001) prior to conducting the experiments with an approval number REC42/1/027. All the procedures were in accordance with the guidelines set by the Organization for Economic Cooperation and Development and International Conference on Harmonization. The results of the experiments were reported in accordance with the ARRIVE 2.0 guidelines.

Synthesis of titled compounds

All the titled compounds were synthesized using the scheme shown in Fig. 1.

Synthesis of 5-(4-substituted benzylidene)-thiazolidine-2,4-diones (2a–e)

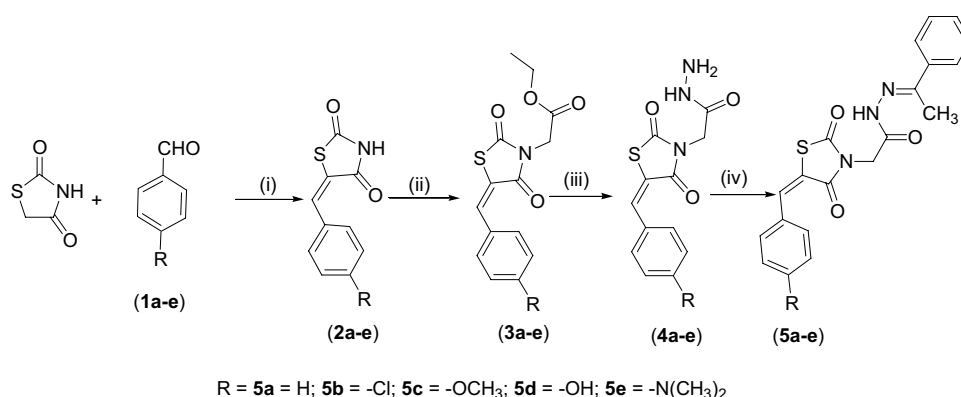
Thiazolidine-2,4-dione (0.25 mol) and an appropriate proportion of aryl aldehydes (0.25 mol) were mixed in 50 mL of hot glacial acid, followed by the addition of fused sodium acetate (1.8 g) to the resulting solution. The reaction mixture was then refluxed for 5 h. The progress of the reaction was continuously monitored using TLC. Upon the completion of the reaction, the reaction mixture was allowed to cool at room temperature and then added to ice-cold water. Thus, a solid product was obtained, filtered, dried, and purified by recrystallization from glacial acetic acid.

Synthesis of [5-(4-substituted-benzylidene)-2,4-dioxothiazolidin-3-yl]acetic acid ethyl esters (3a–e)

Substituted-benzylidene thiazolidine-2,4-diones (**2a–e**, 0.02 mol), ethyl chloroacetate (0.04 mol), and potassium carbonate (0.04 mol) were mixed in acetone (250 mL) and refluxed for 16 h. The inorganic base was filtered off, and the filtrate was evaporated to dryness under reduced pressure using a rotavapor. The obtained solid residue was recrystallized using methanol to afford the corresponding acetates (**3a–e**).

Synthesis of [5-(4-substituted-benzylidene)-2,4-dioxothiazolidin-3-yl]acetic acid hydrazides (4a–e)

Substituted-benzylidene thiazolidine-2,4-dione ethyl esters (**3a–e**, 0.01 mol) were added to hydrazine hydrate (10 mL), then mixed with an appropriate quantity of absolute ethanol (30 mL), and stirred to achieve a clear solution. The resulting solution was refluxed for 7 h. After the reaction was completed, ethanol was concentrated under vacuum to obtain the crude compound, which was then stirred into *n*-hexane, filtered at reduced pressure, and dried. Finally, the obtained desired compound was purified by recrystallization under ethanol.



Reagents and conditions: (i) CH₃COONa, glacial acetic acid, reflux; (ii) ethylchloroacetate, K₂CO₃, acetone; (iii) hydrazine hydrate, absolute ethanol, reflux; (iv) acetophenone, glacial acetic acid, CH₃COONa, absolute ethanol, reflux

Figure 1. Synthetic route to the titled compounds (**5a–e**).

Synthesis of [5-(4-substituted-benzylidene)-2,4-dioxothiazolidin-3-yl]acetic acid (1-phenylethylidene)hydrazides (5a–e)

Equimolar quantities (6 mmol) of substituted-benzylidene thiazolidine -2,4-dione hydrazides (**4a–e**) and acetophenone were dissolved in absolute ethanol (50 mL), followed by the addition of glacial acetic acid (3 mL). The resulting mixture was then refluxed for 10 h, and the progress of the reaction was monitored by TLC using ethyl acetate and petroleum ether (2:1) as solvents. After the reaction was completed, the reaction mixture was cooled to room temperature, concentrated under reduced pressure, and recrystallized using ethanol to afford the corresponding hydrazides as titled compounds (**5a–e**).

[5-(4-Benzylidene-2,4-dioxo-thiazolidin-3-yl)-acetic acid (1-phenyl-ethylidene)-hydrazide (5a)

Color: light brown; Yield: 38%; Melting point (MP): 120–122 °C. FT-IR (KBr, ν , cm^{-1}): 3244(–NH), 3058(Ar–CH), 3005(CH), 2925(CH_2), 1705, 1659, 1602 (C=O), 1556 (C=C), 1492 (C=N); ^1H NMR (500 MHz, $\text{DMSO}-d_6$, δ ppm): 1.72 (s, 3H, CH_3), 4.13 (s, 2H, CH_2), 7.10 (s, 1H, CONH), 7.46 (s, 1H, methylidene C–H), 7.96–7.05 (m, 10H, Ar–H); ^{13}C NMR (100 MHz, $\text{DMSO}-d_6$, δ ppm): 15.9 (CH_3), 40.36 (CH_2), 126.94 (C=C, Thiazolidinedione), 127.1, 127.2, 128.5, 128.7, 128.9, 129.0, 130.2, 130.9, 131.0, 131.3, 135.9, 137.2 (C, Benzene), 137.3 (methylidene C=C), 153.7, 156.2, 159.1 (C=O), 160.1 (C=N); Mass m/z (M + H) $^+$: 380.15; Analysis calculated for $\text{C}_{20}\text{H}_{17}\text{N}_3\text{O}_3\text{S}$: C (63.31); H (4.52); N (11.07); O (12.65); S (8.45); R_f value = 0.75; Log P = 4.31.

[5-(4-Chloro benzylidene)-2,4-dioxo-thiazolidin-3-yl] acetic acid (1-phenyl-ethylidene)-hydrazide (5b)

Color: light brown; Yield: 35%; MP: 115–117 °C; FT-IR (KBr, ν , cm^{-1}): 3334(–NH), 3193(Ar–CH), 3063(CH), 2924(CH_2), 1774, 1682, 1604 (C=O), 1487 (C=C), 1443 (C=N), 759 (C–Cl); ^1H NMR (500 MHz, $\text{DMSO}-d_6$, δ ppm): 2.08 (s, 3H, CH_3), 3.86 (s, 2H, CH_2), 7.91–7.14 (m, 9H, Ar–H), 7.20 (s, 1H, CONH), 7.86 (s, 1H, methylidene C–H); ^{13}C NMR (100 MHz, $\text{DMSO}-d_6$, δ ppm): 15.6 (CH_3), 40.19 (CH_2), 126.93 (C=C, Thiazolidinedione), 127.1, 127.2, 128.7, 128.8, 120.0, 129.1, 130.2, 130.9, 131.0, 131.1, 131.3, 135.6 (C, Benzene), 135.7 (methylidene C=C), 153.7, 157.7, 159.1 (C=O), 160.06 (C=N); Mass m/z (M + H) $^+$: 414.17; Analysis calculated for $\text{C}_{20}\text{H}_{16}\text{ClN}_3\text{O}_3\text{S}$: C (58.04); H (3.90); Cl (8.57); N (10.15); O (11.60); S (7.75); R_f value = 0.70; Log P = 5.02.

[5-(4-Methoxy benzylidene)-2,4-dioxo-thiazolidin-3-yl]-acetic acid (1-phenyl-ethylidene)-hydrazide (5c)

Color: deep brown; Yield: 40%; MP: 112–114 °C; FT-IR (KBr, ν , cm^{-1}): 3343(–NH), 3063(Ar–CH), 2957(CH), 2921(CH_2), 1723, 1683, 1604 (C=O), 1568 (C=C), 1490 (C=N), 1025(C–O–C); ^1H NMR (500 MHz, $\text{DMSO}-d_6$, δ ppm): 2.2 (s, 3H, CH_3), 3.67 (s, 3H, OCH_3), 3.88 (s, 2H, CH_2), 7.92–7.04 (m, 9H, Ar–H), 7.11 (s, 1H, CONH), 7.84 (s, 1H, methylidene C–H); ^{13}C NMR (100 MHz, $\text{DMSO}-d_6$, δ ppm): 15.1 (CH_3), 40.60 (CH_2), 111.46 (C=C, Thiazolidinedione), 112.0, 112.2, 126.3, 126.92, 126.99, 128.6, 128.7, 128.8, 129.1, 129.9, 130.2, 133.6, 137.2 (C, Benzene), 138.3 (methylidene C=C), 152.5 (C=O), 157.7 (C=N); Mass m/z (M + H) $^+$: 410.26; Analysis calculated for $\text{C}_{21}\text{H}_{19}\text{N}_3\text{O}_4\text{S}$: C (61.60); H (4.68); N (10.26); O (15.63); S (7.83); R_f value = 0.64; Log P = 4.23.

[5-(4-Hydroxy benzylidene)-2,4-dioxo-thiazolidin-3-yl]-acetic acid (1-phenyl-ethylidene)-hydrazide (5d)

Color: cream; Yield: 45%; MP: 110–112 °C; FT-IR (KBr, ν , cm^{-1}): 3190(–OH), 3100(–NH), 2950(Ar–CH), 2924(CH), 2849(CH_2), 1720, 1650, 1606 (C=O), 1507 (C=C), 1434 (C=N); ^1H NMR (500 MHz, $\text{DMSO}-d_6$, δ ppm): 1.6 (s, 3H, CH_3), 2.57 (s, 2H, CH_2), 4.12 (s, 1H, OH), 7.90–7.07 (m, 9H, Ar–H), 7.4 (s, 1H, CONH), 7.73 (s, 1H, methylidene C–H); ^{13}C NMR (100 MHz, $\text{DMSO}-d_6$, δ ppm): 21.9 (CH_3), 40.1 (CH_2), 116.17 (C=C, Thiazolidinedione), 115.9, 116.17, 116.5, 122.3, 123.5, 127.12, 131.6, 131.7, 132.0, 132.6, 134.2, 139.0 (C, Benzene), 147.9 (methylidene C=C), 160.3, 165.2, 167.3 (C=O), 174.29 (C=N); Mass m/z (M + H) $^+$: 396.19; Analysis calculated for $\text{C}_{20}\text{H}_{17}\text{N}_3\text{O}_4\text{S}$: C (60.75); H (4.33); N (10.63); O (16.18); S (8.11); R_f value = 0.60; Log P = 3.64.

[5-(4-Dimethylamino benzylidene)-2,4-dioxo-thiazolidin-3-yl]-acetic acid (1-phenyl-ethylidene)-hydrazide (5e)

Color: deep brown; Yield: 50%; MP: 118–120 °C; FT-IR (KBr, ν , cm^{-1}): 3190(–NH), 2975(Ar–CH), 2914(CH), 2801(CH_2), 1760, 1679, 1601 (C=O), 1520 (C=C), 1442 (C=N), 1227 (C–N); ^1H NMR (500 MHz, $\text{DMSO}-d_6$, δ ppm): 2.26 (s, 3H, CH_3), 2.91 (s, 6H, N– CH_3), 4.12 (s, 2H, CH_2), 7.96–7.01 (m, 9H, Ar–H), 7.4 (s, 1H, CONH), 7.70 (s, 1H, methylidene C–H); ^{13}C NMR (100 MHz, $\text{DMSO}-d_6$, δ ppm): 21.9 (CH_3), 40.1 (CH_2), 39.8, 39.9 (N– CH_3), 111.6 (C=C, Thiazolidinedione), 112.9, 113.7, 115.3, 115.9, 116.1, 123.5, 126.8, 127.1, 127.3, 128.5, 128.7, 128.8 (C, Benzene), 131.7 (methylidene C=C), 144.5, 153.9, 155.0 (C=O), 167.0 (C=N); Mass m/z (M + H) $^+$: 423.23; Analysis calculated for $\text{C}_{22}\text{H}_{22}\text{N}_4\text{O}_3\text{S}$: C (62.54); H (5.25); N (13.26); O (11.36); S (7.59); R_f value = 0.60; Log P = 4.47.

Acute oral toxicity test

The acute oral toxicity test of the titled compounds was performed in vivo on male Swiss albino mice (24 ± 2.5 g) using a reported procedure^{12,13}. The mice were fasted for 4 h prior to the administration of the test compounds. The solubility profile of the test chemicals at various dosage levels was determined, and a vehicle consisting of 5% DMSO and distilled water was used. The test chemicals were administered orally at consecutive doses beginning at 10 mg/kg. The second dosage of 50 mg/kg was administered after 48 h, and the animals were observed for symptoms of toxicity, particularly in the first 4 h. The dosage was further increased to 500 mg/kg, and the survival of animals was monitored for 14 days. The test mice were observed for acute poisoning symptoms such as lacrimation, hair erection, blinking, increased urine output, muscular weakness, drowsiness, convulsions, decrease in motor activity, diarrhea, coma, and death.

Oral glucose tolerance test

Oral glucose tolerance test (OGT) was performed on male Swiss albino mice weighing 24 ± 2.5 g¹⁴. After a 16 h fast, each mouse had their blood glucose level (BGL) checked, and those with BGLs between 60 and 90 mg/dL were divided into 12 groups of six mice each. The mice in the experimental groups were given oral doses of 50 mg/kg and 100 mg/kg body weight of synthesized chemicals dissolved in 5% DMSO. The same amount of DMSO was given to the test, positive control, and negative control group. Rosiglitazone (12.5 mg/kg body weight) was administered orally to the positive control group. A glucose load (2.5 g/kg body weight) was given orally to each animal 30 min after the test sample or vehicle was administered. The blood glucose profile of each mouse was measured using a glucometer at 0, 30, 60, 90, and 120 min after glucose administration. The BGL of each mouse was assessed three to four times, and the average was calculated. During the trial, the cages were devoid of food but not of water. OGT was used to screen the test compounds for hypoglycemic action in normal, healthy mice at two dosage levels (50 and 100 mg/kg body weight) to establish the therapeutic dose. For future studies, the dosage that improves glucose tolerance in a similar way to the standard drug was chosen.

In vivo antidiabetic activity

DM was induced in the mice through a single intraperitoneal (i.p.) injection of nicotinamide and streptozotocin (STZ)^{15,16}. First, nicotinamide was dissolved in normal saline and administered at a dose of 120 mg/kg body weight into the mice fasted overnight. At 15 min post nicotinamide administration, STZ was injected intraperitoneally at 60 mg/kg body weight dose. The STZ solution (0.1 M, pH 4.5) was prepared fresh by dissolving an appropriate amount of STZ in citrate buffer. The fasting blood glucose (FBG) level was measured after 72 h in each mouse by taking the blood samples from the tail vein using a glucometer. Each mouse's BGL was monitored three to four times, and only those with average BGL over 200 mg/dL were chosen for the study and designated as STZ-induced diabetic animals.

The selected STZ-induced diabetic mice were weighed again before the study and split randomly into seven groups with six animals each. Group 1, the diabetic control group, was orally given 5% DMSO only as vehicle. Group 2 served as the positive control group and was given the standard drug rosiglitazone. Groups 3–7 orally received the synthesized compounds (5a–e) dissolved in DMSO. All the animals were fasted overnight, and their FBG levels on day 0 were determined. The test compounds were administered individually to the assigned groups at a dose of 100 mg/kg orally every day at a fixed time for 21 days. The vehicle was given to the negative control group, and rosiglitazone was administered at a dosage of 12.5 mg/kg body weight to the positive control group. Blood samples were withdrawn on days 0, 7, 14, and 21 from all the animals, and the percentage decrease in FBG was determined. On each sampling day, blood samples were collected from the tail vein of each mouse 3–4 times, and the average FBG was calculated.

Effect on body weight

For 21 days, all the test compounds were orally administered at 100 mg/kg dose, and standard rosiglitazone was administered at 12.5 mg/kg daily at the same time to the diabetic mice. Their effects on body weight was studied relative to the body weight of the diabetic control.

Molecular docking study

The 3D structure of PPAR- γ bound with its partial agonist nTZDpa (PDB ID: 2Q5S) was downloaded from the Research Collaboratory for Structural Bioinformatics database (<https://www.rcsb.org>). Chain A was deleted, and chain B was used for processing the receptor structure for docking. The binding coordinates of the native ligand nTZDpa were marked and retained for binding site identification. After the removal of native ligand and solvent, the receptor was energy-minimized by applying Amber ff14SB force field for standard residues and Gasteiger charges for other residues in Chimera 1.13.1¹⁷. The prepared receptor was saved in *.pdbqt format for further use. The structures of ligands under investigation were drawn in ChemDraw and saved in protein data bank (PDB) format. The native ligand nTZDpa structure for redocking was retrieved from PubChem in SMILES format. All ligand structures were processed in Chimera to obtain a minimum energy conformer through 100 steepest descent steps with the step size of 0.02 Å, followed by 10 conjugate gradient steps of size 0.02 Å. The stabilized ligand conformers were also saved in *.pdbqt format.

Molecular docking was carried out in Chimera-based AutoDock Vina. The docking grid was set up around the binding site. This grid box has dimensions centered at $35 \times 8 \times 40$ Å and a size $20 \times 20 \times 20$ Å corresponding to the X, Y, and Z axes. The docking protocol searched for a maximum of 10 conformers per ligand at an energy difference of 3 kcal/mol, with exhaustiveness of search set at 8. Ligand conformers were then ranked according to their predicted binding energy. The conformer with the minimum binding energy was chosen as the best conformer and retained for further binding interaction analysis. The investigated ligands were manually ordered based on their binding energies: the compound with the highest negative value for binding was the best active compound. The reliability of the developed docking protocol was verified by redocking the native ligand nTZDpa to 2Q5S. The standard deviation between the conformers of the native ligand and the redocked native ligand was an indication of reliability: the lower the root-mean-square deviation (RMSD), the higher the reliability. The docked complexes of 2Q5S were probed for the intermolecular binding interactions in Discovery Studio.

Protein–ligand interaction-based pharmacophore model analysis

The 3D pharmacophore model was analyzed with LigandScout 4.3 software using the 3D structures of 2Q5S docked to compounds 5c and 5d. The 3D pharmacophore model was generated for compound 5c first by loading the corresponding docked complex onto the macromolecular view. The ligand was then checked for missing bonds, if any, by focusing on the yellow box on the ligand. Afterward, the 3D pharmacophore model was created

by selecting the create model option. The ligand and the pharmacophore model were saved to the alignment mode. The 3D structure of 2Q5S complexed with compound **5d** was then loaded, and the procedure was repeated. Both pharmacophore models from compounds **5c** and **5d** were aligned, and the fingerprint features were shared and merged to create a 3D pharmacophore model with merged structural features¹⁸.

Molecular dynamics simulation studies

MD simulation was used to examine the thermodynamic behavior and stability of the best-ranked conformation of compound **5c** in contact with PPAR- γ provided by the docking study. We used the Desmond 7.4 software integrated with Maestro of Schrödinger, Inc. (<https://www.schrodinger.com/products/desmond>) for MD. To better understand the conformational changes caused by the test ligand binding, the apo form of the PPAR- γ and native partial agonist nTZDpa-PPAR- γ complex were also simulated. Inside an orthorhombic box with a 10 Å buffer region between protein atoms and box sides, the apo form of PPAR- γ and compound **5c**-PPAR- γ or nTZDpa-PPAR- γ complexes were inserted. The box was then filled with the required number of water molecules in accordance with the system setup procedure.

A simple point charge (SPC) model and OPLS3e force field were adopted for the MD computations¹⁹. The system was neutralized with an appropriate number of Na⁺ and Cl⁻ ions, at a salt concentration of 0.15 M, which reflects monovalent ion concentration in the body. The temperature and pressure were set to 300 K and 1.01325 bar, respectively, using an isothermal-isobaric (NPT) ensemble. The simulation time was customized to 150 ns, and trajectories were recorded every 150 ps. For short-range van der Waals and Coulomb interactions, a cut-off radius of 9.0 was chosen. The system temperature and pressure were maintained using the Nose-Hoover thermostat and Martyna-Tobias-Klein techniques, respectively. For bonded and non-bonded interactions inside the short-range cut-off, the reversible reference system propagator algorithm (RESPA) integrator was employed with an inner time step of 2.0 fs to integrate the equations of motion. The system was minimized and equilibrated to Desmond's default protocols. The Desmond package's simulation interaction diagram module was used to examine the trajectory files.

Statistical analysis

The data obtained for the antidiabetic activity using the in vivo STZ-induced diabetic model and the effect of synthesized compounds on the body weight were analyzed by two-way mixed analysis of variance (ANOVA) using RStudio program version 1.4.1564 (Posit, PBC, Vienna, Austria). The mean \pm standard error of the mean (SEM) values were compared and cross-classified by two independent categorical variables, including one between the groups and one within the group. Values (p) < 0.05 were significant.

Results and discussion

Synthesis

New [5-(4-substituted-benzylidene)-2,4-dioxothiazolidin-3-yl]acetic acid (1-phenylethylidene)hydrazides (**5a-e**) were synthesized first by reacting thiazolidine-2,4-dione and appropriate aromatic aldehydes (**1a-e**) to afford compounds 5-(4-substituted-benzylidene)-thiazolidine-2,4-diones (**2a-e**). The corresponding ethyl esters (**3a-e**) were then synthesized by reacting benzylidene-thiazolidine-2,4-diones (**2a-e**) with ethyl chloroacetate. The substituted [5-(4-substituted-benzylidene)-2,4-dioxothiazolidin-3-yl] acetic acid hydrazides (**4a-e**) were synthesized by refluxing the ethyl esters (**3a-e**) with hydrazine hydrate. Finally, the target benzylidene-2,4-thiazolidinediones (**5a-e**) were synthesized by reacting the acetic acid hydrazides (**4a-e**) with acetophenone.

All the synthesized compounds were characterized using various spectral techniques such as FT-IR, ¹H-NMR, ¹³C-NMR, and MS. The structures of all the synthesized compounds were supported by their physicochemical properties and spectral characteristics. The FT-IR spectra of the titled compounds showed characteristic bands at 3190 (–OH), 3343–3100 (–NH), 3193–2950 (Ar–CH), 3063–2914 (CH), 2925–2801 (CH₂), 1774–1601 (C=O), 1568–1487 (C=C), 1492–1434 (C=N), 1227 (C–N), 1025 (C–O–C), and 759 (C–Cl). The ¹H-NMR spectra confirmed the presence of –CH₃, –CH₂, CONH, and –C–H groups by showing singlets at δ 1.6–2.26, δ 2.57–4.13, δ 7.1–7.4, and δ 7.46–7.86 ppm, respectively. Meanwhile, the Ar–H groups were confirmed by detecting multiplets at δ 7.96–7.01 ppm. Singlets for –OCH₃ and OH were observed at 3.67 and 4.12 ppm, respectively. The ¹³C-NMR spectra confirmed the presence of –CH₃, –CH₂, C=C (thiazolidinedione), C (benzene), methyldene (C=C), and (C=N). Electrospray ionization (ESI) in MS revealed the protonated molecular ions in the positive ion mode. Mass m/z (M + H)⁺ peaks at 380.15, 414.17, 410.26, 396.19, and 423.23 were observed for compounds **5a**, **5b**, **5c**, **5d**, and **5e**, respectively.

Acute toxicity test

The acute oral toxicity test was performed to evaluate the acute physical, fatal, or behavioral changes caused by the newly synthesized compounds when administered orally. The synthesized benzylidene-2,4-thiazolidinedione (**5a-e**) derivatives were administered in a series of doses ranging 10–500 mg/kg, followed by the measurement of weight before and after the treatment. The mice were monitored for 14 days and exhibited no symptoms of harm. Furthermore, no deaths occurred throughout the follow-up study. No significant variation in mouse weight was observed pre- and post-treatment, indicating the median lethal dose (LD₅₀) of each compound to be more than 500 mg/kg.

Oral glucose tolerance test

The blood glucose lowering action of each benzylidene-2,4-thiazolidinedione (**5a-e**) derivative was evaluated at 50 and 100 mg/kg doses in normal mice, and the results are summarized in Table 1. The blood glucose concentration was measured at six time points: 30 min before administering the test compounds, immediately before

Group	Dose (mg/kg)	Percent decrease in BGL				
		0 min	30 min	60 min	90 min	120 min
Rosiglitazone	12.5	8.0 ± 1.4	35.2 ± 3.8	36.9 ± 3.9	39.4 ± 2.7	41.9 ± 3.9
5a	50	3.3 ± 0.5	28.4 ± 3.1	35.4 ± 4	38.7 ± 3.8	41.5 ± 2.2
	100	6.78 ± 0.9	29.8 ± 3.3	38.7 ± 3.9	43.1 ± 0.7	45.2 ± 1.5
5b	50	1.9 ± 0.5	18.5 ± 4.4	19.6 ± 4.6	20 ± 4.7	22.5 ± 4.1
	100	3.8 ± 0.3	19.6 ± 1.2	24.2 ± 1.8	25.4 ± 1.9	27.8 ± 1.5
5c	50	2.6 ± 0.2	22.1 ± 3.4	32.4 ± 3.7	38.4 ± 2.8	43.4 ± 2.9
	100	5.9 ± 0.7	28.4 ± 3.6	42.6 ± 3.7	47.2 ± 3.5	48.8 ± 3.9
5d	50	1.0 ± 0.2	13.9 ± 1.3	17.9 ± 2.3	19.4 ± 1.9	22.0 ± 2.5
	100	1.9 ± 0.9	18.7 ± 1.7	24.8 ± 2.5	26.4 ± 2.3	30.1 ± 2.8
5e	50	6.5 ± 1.0	30.7 ± 3.4	34.2 ± 4.2	40.3 ± 2.3	44.8 ± 3.6
	100	7.4 ± 1.2	43.9 ± 2.8	45.4 ± 4.2	53.3 ± 12.3	59.8 ± 16.6

Table 1. Postprandial glucose lowering effects (%) of test compounds on normal mice post-glucose load.

the glucose loading (0 min), and 30, 60, 90, and 120 min after the glucose administration. Compared with the control, all the tested compounds exhibited remarkable reductions in BGL at both doses (Table 1). All the tested compounds and the standard drug rosiglitazone caused a steady decrease in BGL as evident from the increasing percentage decrease in BGL with time. In particular, compound 5e at 100 mg/kg dose showed the greatest percent decrease (59.79%) in mice at 120 min. This percent decrease was even higher than that for the standard drug rosiglitazone (41.90%) tested at 12.5 mg/kg dose after 120 min. Table 1 shows that the postprandial glucose-lowering effects of all the tested compounds were dose and time dependent.

In vivo antidiabetic activity

The in vivo antidiabetic screening of synthesized benzylidene-2,4-thiazolidinediones (5a–e) were performed on the STZ-induced diabetic murine model. The test compounds (100 mg/kg) and rosiglitazone (12.5 mg/kg) were administered to the diabetic mice for 21 days at a set time each day. FBG levels were measured at the same time on days 0, 7, 14, and 21, and the findings are presented in Table 2. Compared with the control, all the test compounds caused a substantial decrease in FBG on days 7, 14, and 21 in a manner similar to the standard drug rosiglitazone. As evident from the lowest FBG, the maximum antidiabetic activity as was observed at day 21 for all the test compounds and rosiglitazone. Among the test compounds, the best antidiabetic activity was discovered for compound 5d (% decrease = 59.28%), followed closely by 5e (% decrease = 55.67%).

Statistically significant two-way interactive effects were observed between treatment group and time on FBG with $F(18, 42) = 31.4$ and $p < 0.0001$. Pairwise comparison between groups at each time revealed that all the test compounds induced a highly significant ($p < 0.0001$) reduction in BGL comparable with the standard drug rosiglitazone. The maximum percent change in FBG level was observed with compounds 5d (59.28%) and 5e (55.67%). Furthermore, a pairwise comparison was performed between different times within groups to investigate the effects of treatment and time on the FBG, and the findings are depicted in Figs. 2 and 3. The mean FBG values were significantly different in the control versus treatment groups at all time points.

Effects on the body weight of STZ-induced diabetic mice

The effects of the test compounds (5a–e) and the standard drug rosiglitazone on the body weight of STZ-induced diabetic animals were studied for 21 days, and the results are presented in Table 3. Rosiglitazone induced a slight increase in body weight at the end of the study period, and all the test compounds did not cause any changes in body weight. This finding showed that the synthesized compounds did not cause any considerable weight gain in the treated animals.

Group	FBG (mg/dL)				% change (Day 21–Day 0)
	Day 0	Day 7	Day 14	Day 21	
Diabetic control	265.7 ± 17.2	302.9 ± 18.9	319.9 ± 24	345.7 ± 12.4	30.1 ± 13.4
Rosiglitazone	269.7 ± 2.1	191.0 ± 9.5****	161.7 ± 7.8****	130.7 ± 1.5****	51.5 ± 0.7
5a	287.0 ± 6.1*	195.7 ± 7.0****	167.0 ± 3.6****	132.3 ± 5.5****	53.9 ± 1.7
5b	273.3 ± 6.8	206.0 ± 14.7****	174.3 ± 10.2****	125 ± 6.6****	54.2 ± 3.0
5c	272.3 ± 16.9	210.0 ± 15.7****	164 ± 19.1****	124.3 ± 5.7****	54.4 ± 4.8
5d	298 ± 14**	194.3 ± 5.0****	158.7 ± 9.5****	121.3 ± 4.5****	59.3 ± 1.8
5e	285.0 ± 8.5	207.3 ± 16.8****	169.0 ± 2.7****	126.3 ± 5.5****	55.7 ± 1.0

Table 2. Effect of test compounds (5a–e) and rosiglitazone on the FBG of STZ-induced diabetic mice. * $p < 0.05$; ** $p < 0.01$; *** $p < 0.001$; **** $p < 0.0001$.

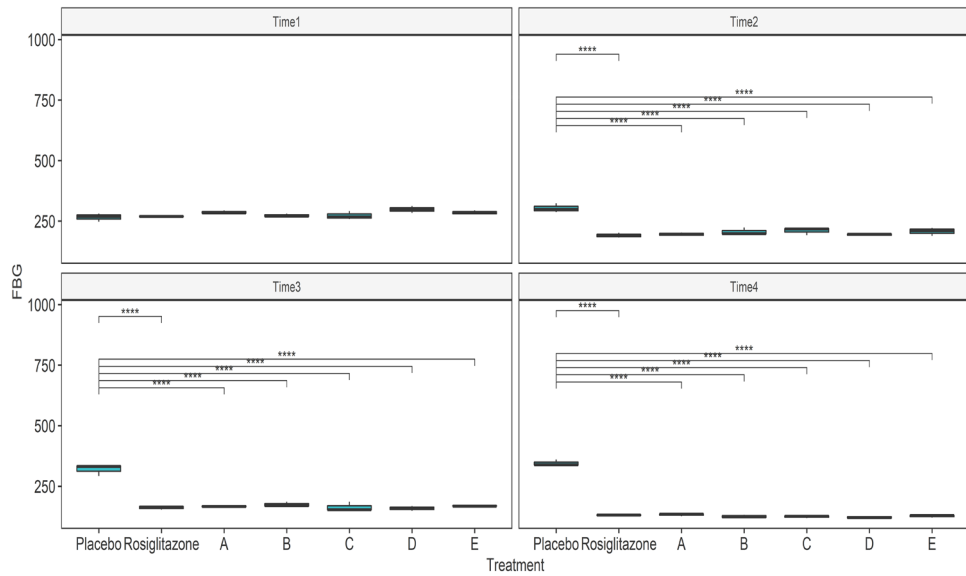


Figure 2. Pairwise comparison between different time points within treatment groups. Time 1, Time 2, Time 3, and Time 4 represents 0, 7, 14, and 21 days respectively; placebo = diabetic control; treatment A, B, C, D, and E represent test compounds 5a, 5b, 5c, 5d, and 5e, respectively; **** $p < 0.0001$.

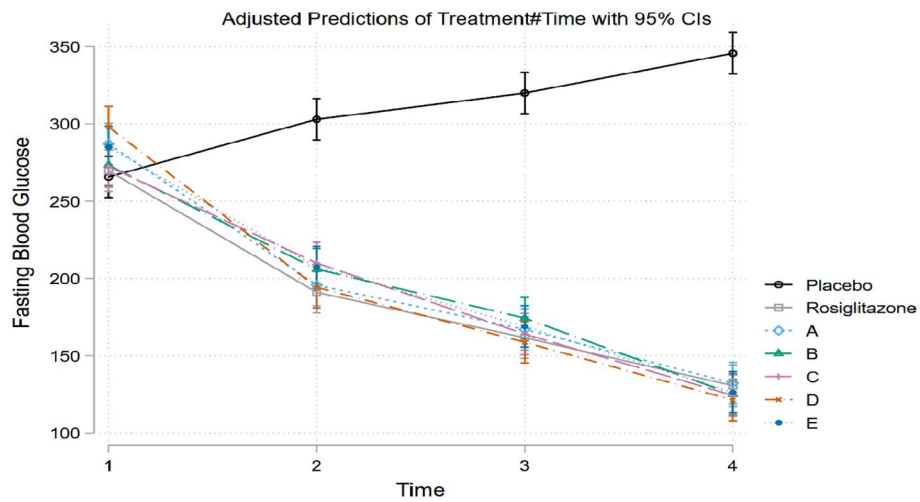


Figure 3. Graph showing effects of standard rosiglitazone and test compounds in FBG in comparison to the control. Placebo = diabetic control; treatment A, B, C, D, and E represent test compounds 5a, 5b, 5c, 5d, and 5e, respectively.

Group	Body weight (g)				% change (Day 21–Day 0)
	Day 0	Day 7	Day 14	Day 21	
Diabetic control	25.0 ± 0.6	24.8 ± 0.3	23.7 ± 0.3	22.3 ± 0.9	−10.9 ± 1.2
Rosiglitazone	25.5 ± 0.4	26.0 ± 0.67*	26.8 ± 0.4****	27.5 ± 0.5****	7.7 ± 0.8
5a	25 ± 0.6	25.3 ± 0.4	26.0 ± 0.4**	25.9 ± 1.0***	3.5 ± 0.4
5b	24.6 ± 0.3	24.5 ± 0.2	24.0 ± 0.1	23.8 ± 0.2	−3.3 ± 0.5
5c	24.9 ± 0.3	24.6 ± 0.3	24.7 ± 0.4*	24.3 ± 0.4*	−2.5 ± 0.5
5d	24.2 ± 0.3	24.5 ± 0.2	24.7 ± 0.1*	25.1 ± 0.1**	3.5 ± 0.7
5e	24.7 ± 0.2	24.6 ± 0.2	24.8 ± 0.3*	24.8 ± 0.2**	0.9 ± 0.2

Table 3. Effects of test compounds on the body weight of STZ-induced diabetic mice. * $p < 0.05$; ** $p < 0.01$; *** $p < 0.001$; **** $p < 0.0001$.

The results of treated groups were statistically compared with those of the diabetic control group and the change in body weight was compared at each time point within and between the groups. The adjusted predictions are shown in Fig. 4, where the changes in the body weight in each group of animals are also presented. The untreated diabetic control mice showed a decreased body weight throughout the tested period, and those treated with the standard drug rosiglitazone showed an increased body weight.

The change in body weight induced by the test compounds was examined relative to the body weight of the control at different time points to determine the level of significance. None of the test compounds induced any significant difference in body weight compared with that of the control after 7 days; however, rosiglitazone caused a statistically significant ($*p < 0.05$) change in body weight relative to that of the control at this time. This effect continued after 14 days, with rosiglitazone inducing a highly significant ($****p < 0.0001$) change in body weight due to its opposite effects on body weight over time. For the test compounds, compound **5a** caused a significant ($**p < 0.01$) change in body weight relative to the control after 14 days. Compounds **5c**, **5d**, and **5e** also induced lesser but statistically significant changes in body weight ($*p < 0.05$) compared with that of the control. At the end of the study period (21 days), the level of significance for compounds **5d** and **5e** increased ($**p < 0.01$), and a similar trend was observed for compound **5a** ($***p < 0.001$) after 21 days.

Molecular docking study

The applied molecular docking protocol was successful in predicting the bioactive conformations of all investigated ligands. As shown in Fig. 5, the RMSD between the native and redocked native ligands was calculated to be 0.368 Å, indicating that the docking protocol was reliable. Figure 6 shows that all the titled compounds (**5a–e**)

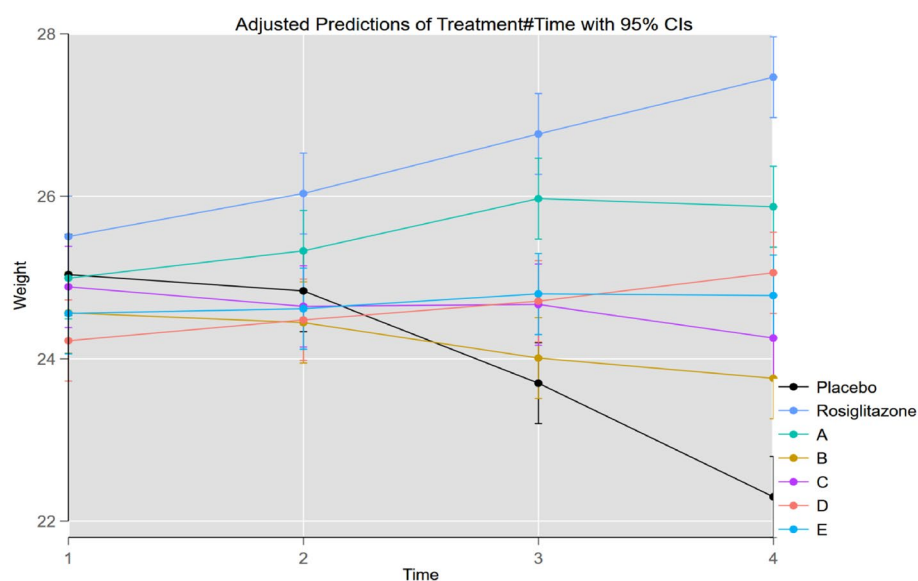


Figure 4. Change in animal body weight in different groups at time 1 (day 1), time 2 (day 7), time 3 (day 14) and time 4 (day 21). Placebo = diabetic control; treatment A, B, C, D, and E represent test compounds **5a**, **5b**, **5c**, **5d**, and **5e**, respectively.

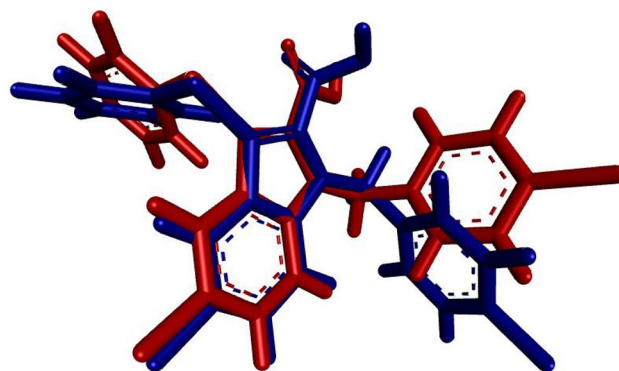


Figure 5. Superimposed native and re-docked native ligand conformations, RMSD (=0.368) value indicated the reliability of the docking protocol.

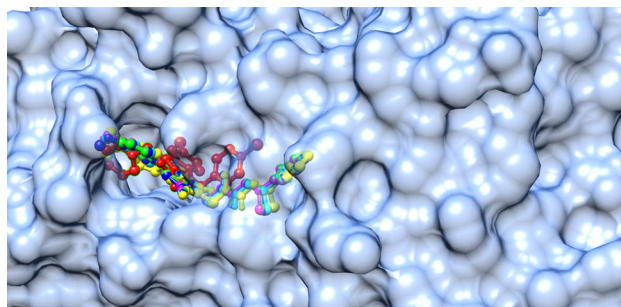


Figure 6. Native ligand (red); **5a** (green); **5b** (cyan); **5c** (blue); **5d** (magenta); and **5e** (yellow) engaged the same binding site of PPAR- γ .

under investigation engaged the same binding site as the native ligand nTZDpa, a partial agonist. Compounds **5c** and **5d** were predicted to exhibit better binding affinities to PPAR- γ than the native ligand as shown in Table 4.

The binding interactions of the native and the top two ligands (**5c** and **5d**) were probed further to understand the nature of these binding interactions and the role of the ligand's structural motifs in enhancing the binding to PPAR- γ . Figure 7A–C display the 2D interactions of the native ligand and compounds **5c** and **5d**, respectively.

PPAR- γ full agonists interact and stabilize the helix-12; however, partial agonists bind to alternative binding sites such as the helix 3 and β -sheet of the PPAR- γ ligand-binding domain²⁰. The foremost interactions for a PPAR- γ partial agonist are hydrogen bonds with Ser342 of β -sheet, Arg288 of helix-5, hydrophobic interactions with Ile341 of β -sheet, and van der Waals interactions with the Cys285 of the helix 3 of PPAR- γ ligand-binding domain. The main difference observed between nTZDpa and compounds **5c** and **5d** was that the hydrophobic interactions contributed chiefly to nTZDpa binding, and the hydrogen bonds contributed significantly to the binding of compounds **5c** and **5d** to PPAR- γ . This finding suggested that the hydrogen bonds were involved in the binding of the test compounds to the protein, resulting in their lower binding energy than nTZDpa. All the characteristic features of partial agonist binding were predicted to be involved in the binding of compounds **5c** and **5d**. These compounds attained an extended conformation inside the binding site, facilitating the electrostatic hydrogen bonds with Arg288 rather than Ser342. The keto oxygen atom of the TZD ring played a crucial role in the binding to Arg288. Two π -donor hydrogen bonds were established with Ser342 by the heterocyclic thiazolidine ring and a keto group, elucidating the importance of the thiazolidinone ring in the receptor binding and its partial agonistic property. This interaction was in accordance with a recent report on PPAR- γ partial agonists²¹.

Hydrophobic interactions with Arg288, Ala292, Ile326, Met329, and Ile341 and van der Waals interactions with Cys285, Leu330, and Leu333 also significantly influenced the binding and partial agonist activity of the test compounds. The phenolic oxygen in compounds **5c** and **5d** participated in hydrogen bonding with His266, which was absent in the case of nTZDpa. The investigated compounds did not occupy the newly identified diphenyl pocket on the PPAR- γ ligand-binding domain²¹. Both compounds displayed similar interactions with PPAR- γ , except the van der Waals interaction of the methyl ether in compound **5c** with Leu255 residue. The hydrogen bond interactions of **5c** and **5d** with His266 were intriguing because the nTZDpa analog BVT.13 has been shown to interact in a similar manner with His266 and BVT.13. This partial agonistic activity is not dependent on H12 binding or stabilization but on the stabilization of β sheet²². Moreover, docking results indicated that compounds **5c** and **5d** did not engage the highly motile binding pocket surrounding $\beta 1$, H2, Ω -loop, and $\beta 2$ – $\beta 4$ sheets made up of the residues Phe247, Ile249, Ile341, Gly344, Gly346, Met348, Thr349, and Arg350. Binding to the abovementioned binding site resulted in the hyperactivation of PPAR- γ ²³. Therefore, compounds **5c** and **5d** were identified as partial agonists of PPAR- γ .

The structure–activity relationship deduced from docking suggested that the conversion of the phenol (**5d**) to its methyl ether derivative (**5c**) slightly increased the binding affinity. However, similar electrostatic hydrogen bond interactions with the receptor were predicted because the oxygen atom of these groups was essential for the formation of hydrogen bond as the hydrogen bond acceptor, not the donor hydrogen. Chlorine (**5b**) and dimethylamino (**5e**) substituents on the phenyl ring did not improve the binding affinity. The thiazolidine ring

Compound ID	Binding energy (ΔG : kcal/mol)	RMSD (Å)
nTZDpa (native ligand)	–9.8	0.368
5a	–9.8	0.767
5b	–9.7	0.788
5c	–10.1	0.721
5d	–10.0	0.730
5e	–8.3	0.794

Table 4. Results of docking benzylidene-2,4-thiazolidinedione derivatives (**5a–e**) to PPAR- γ .

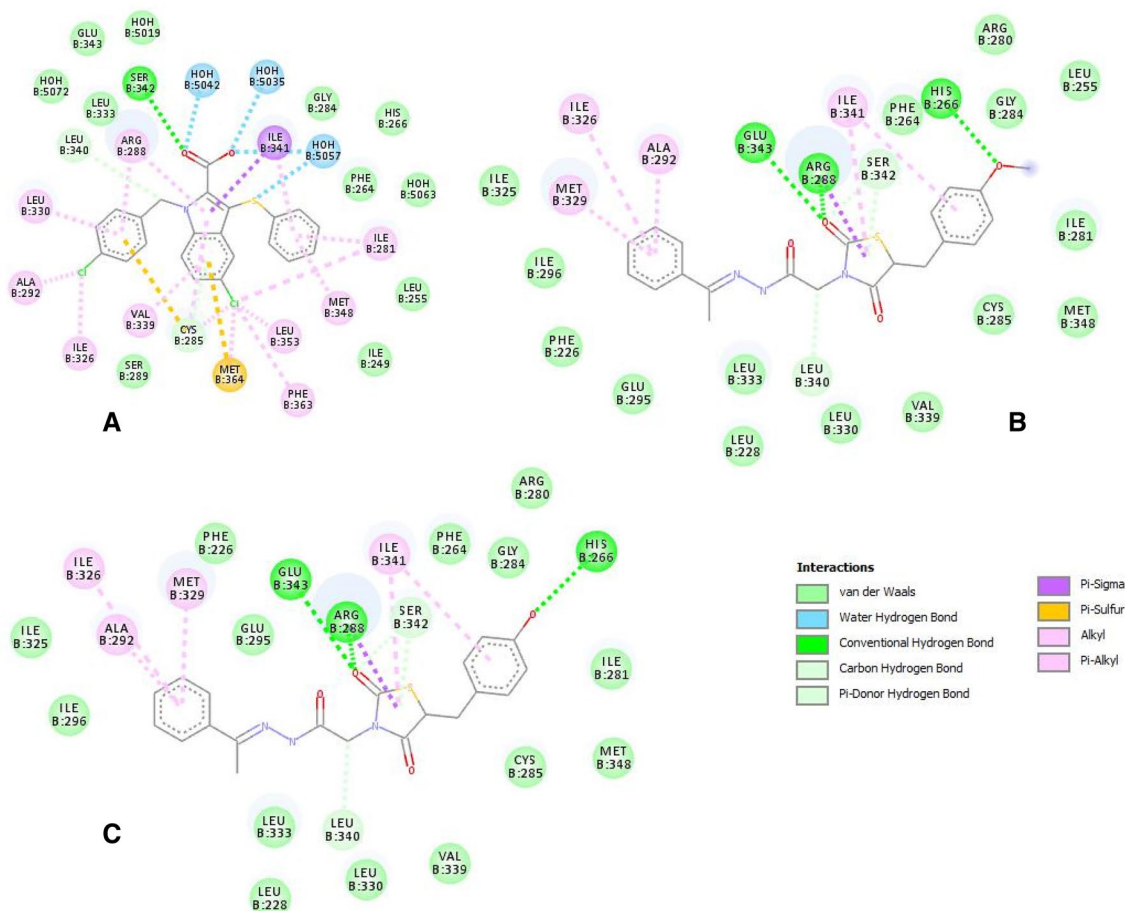


Figure 7. Two-dimensional interaction diagrams of (A) nTZDpa, partial agonist; (B) compound 5c; (C) compound 5d with PPAR- γ .

and a keto group on the thiazolidine ring were important for binding to the receptor. The two terminal aromatic phenyl rings also played a crucial role in the PPAR- γ partial agonistic activity of 5c and 5d. The prototype of antihyperglycemic drugs is TZDs such as rosiglitazone and pioglitazone, which act as full agonists of the PPAR- γ receptor. However, they suffer from the disadvantages of causing heart failure, weight gain, edema, and obesity as side effects. PPAR- γ partial agonists are beneficial over full agonists because they exhibit the dose-related weak transactivation of the receptor by binding to different binding sites and utilizing different coactivators, leading to their distinguished effects²⁴. Molecular docking results suggested that the partial PPAR- γ agonistic activity of compounds 5c and 5d were better than that of the native ligand. These findings were in good correlation with the *in vivo* results supporting the successful design of novel benzylidene 2,4-thiazolidinedione derivatives as PPAR- γ partial agonists for type 2 DM.

Protein–ligand interaction-based pharmacophore model analysis

A 3D pharmacophore model based on protein–ligand interaction summarizes the structural features that are unique to the active conformation of the ligand bound to the binding site of the protein in a 3D space¹⁹. Figure 8 shows the 3D pharmacophore model generated from the characteristic structural features of compounds 5c and 5d. The generated 3D fingerprint may be considered as the lead structure that defines the pharmacophoric features necessary for partial PPAR- γ agonist activity. One hydrogen bond acceptor moiety and two hydrophobic moieties are essential for partial PPAR- γ agonism. The model also illustrated the distance and steric constraints between the protein and ligand. In the Ligand Scout software, the default distance constraint was 2.2–3.8 Å for hydrogen bond interactions and 1.0–5.9 Å for hydrophobic interactions. The rings around the structural features represent the exclusion coat that depicts the sterically forbidden area inside the binding pocket. Pharmacophore models are used as filters in high-throughput virtual screening²⁵. Thus, this study created a 3D pharmacophore model with potential applications in the discovery of PPAR- γ partial agonists.

Molecular dynamic simulation studies

The stability of intermolecular interactions between PPAR- γ and compound 5c was investigated using MD simulation. The conformation of the compound 5c–PPAR- γ complex with the lowest binding energy in the docking experiment was chosen. As a control, PPAR- γ protein in an unbound state and native partial agonist

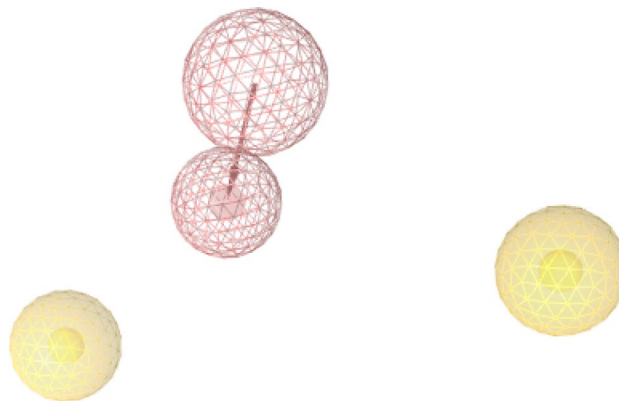


Figure 8. 3D protein–ligand interaction-based pharmacophore model generated from the binding modes of newer benzylidene-2,4-thiazolidinediones. The pink colour depicts a hydrogen bond interaction through an acceptor group and the yellow colour depicts the hydrophobic interactions.

nTZDpa-PPAR- γ complex were also simulated for comparative analysis. The structural stability of the compound 5c and PPAR- γ protein complex was evaluated by computing the root-mean-square deviations (RMSD) and root-mean-square fluctuations (RMSF) of the protein backbone atoms, as shown in Fig. 9. Compound 5c-PPAR- γ complex had an average RMSD value of 2.31 Å, whereas the nTZDpa-PPAR- γ complex and the unbound PPAR- γ protein exhibited an average RMSD value of 2.87 Å and 2.27 Å, respectively. The RMSD results demonstrated greater fluctuation of the nTZDpa-PPAR- γ complex than the compound 5c-PPAR- γ complex (Fig. 9A). The RMSD of compound 5c indicated that it achieved a stable conformation starting from 70 ns and retained stability up to 150 ns of MD simulation.

The fluctuations of apo and compound 5c or nTZDpa-bound protein structures were calculated on a residue basis by selecting carbon-alpha atoms. The Root mean square fluctuation (RMSF) illustrates the dynamics of each atom moving because of numerous hydrogen and hydrophobic connections with nearby residues. The unique conformational modes of interactions are a result of the position variation of the ligand molecules. As seen in

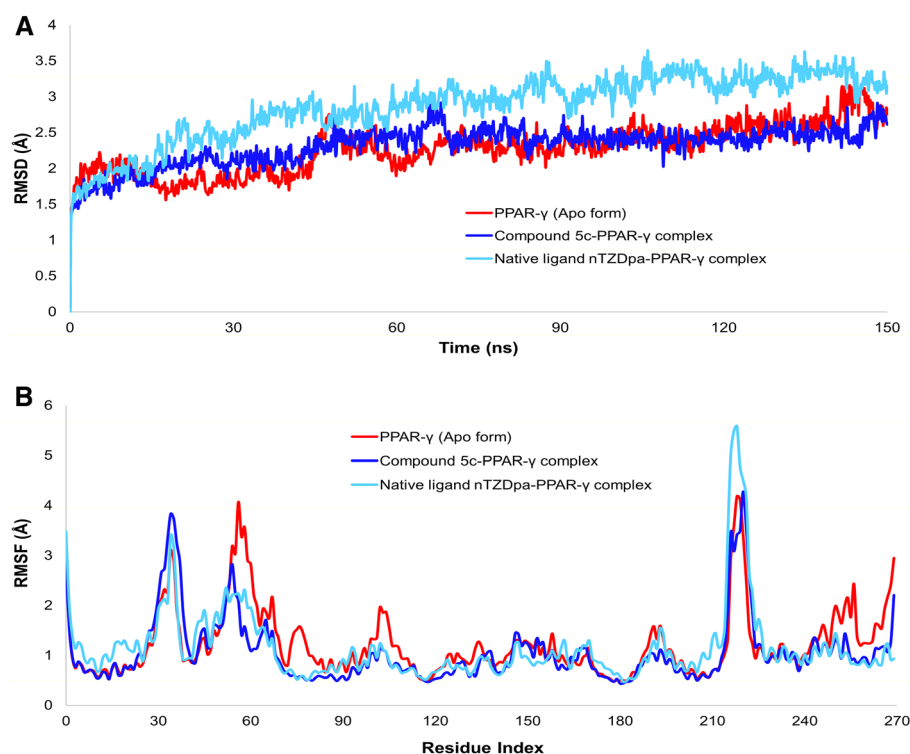


Figure 9. (A) RMSD of Ca atoms of PPAR- γ in apo form (red line) and in complex with compound 5c (blue line) or nTZDpa (sky blue line); (B) RMSF of Ca atoms of PPAR- γ in apo form (red line) and in complex with compound 5c (blue line) or nTZDpa (sky blue line) during 150 ns MD simulation.

Fig. 9B, the RMSF plot of the compound 5c-PPAR- γ complex exhibited less fluctuation and a more stable assembly than the apo or nTZDpa-PPAR- γ complex. The average RMSF values for the apo form and protein-ligand complexes of compound 5c and nTZDpa were calculated to be 1.23 Å, 1.07 Å and 1.17 Å, respectively, for all amino acids of PPAR- γ protein over 150 ns simulated trajectories.

The root mean square distance between the center of mass of each atom in the protein backbone is used to calculate the radius of gyration (rGyr). The rGyr of the compound 5c-PPAR- γ complex concerning the protein backbone is shown in Fig. 10A. The greater spreading area of the protein backbone's atoms accounts for the higher gyration values. The lower rGyr value, on the other hand, denotes the compactness of the protein backbone structure and the stability of the complex. The values of rGyr range between 4.70 and 6.46 Å in compound 5c-PPAR- γ complex whereas the rGyr ranged between 4.24 and 4.56 Å for nTZDpa-PPAR- γ complex, as shown in Fig. 10A, suggesting a stable and compact binding of compounds to PPAR- γ . The solvent-accessible surface area (SASA) of a protein is determined by the surface area accessible to the surrounding solvent molecules, which represents the state of folding compactness or unfolding, affecting the complex's stability. Figure 10B shows the SASA values for the compound 5c-PPAR- γ complex as a function of time.

Figure 11 summarizes the intermolecular interaction fractions of compound 5c and the native ligand nTZDpa with PPAR- γ . More number of hydrogen bonds and hydrophobic interactions were predicted in compound 5c-PPAR- γ complex than in nTZDpa-PPAR- γ complex. Furthermore, the nature of binding interactions and their stability were analyzed from the extracted trajectories of MD. The 2D depiction of binding interactions in compound 5c-PPAR- γ complex and nTZDpa-PPAR- γ complex is shown in Figs. 12 and 13, respectively.

Figure 12 reveals the involvement of solvent bridges in facilitating polar hydrogen bond interactions between compound 5c and PPAR- γ , which docking failed to predict. Moreover, MD unveiled a hydrogen bond interaction between keto oxygen of thiazolidinedione moiety and Ser342 alike nTZDpa. There are slight differences in the binding role of polar functional groups of compound 5c and the binding residues of PPAR- γ predicted in docking and MD, but the number of hydrogen bonds predicted by docking and MD correlated well. The hydrogen bonds formed by compound 5c with Cys285, Leu340, and Ser342 were stable and existed for 54%, 44%, and 29% of the time of MD. Figure 13 shows the stability of one hydrogen bond formed by nTZDpa with Ser342 (14% of the time) and two hydrogen bonds with Glu343 (51% of the time).

The supplementary Fig. S1, is the timeline graph delineating the interactions such as H-bonds, hydrophobic, ionic, and water bridges between compound 5c and PPAR- γ residues during the simulation period of 150 ns.

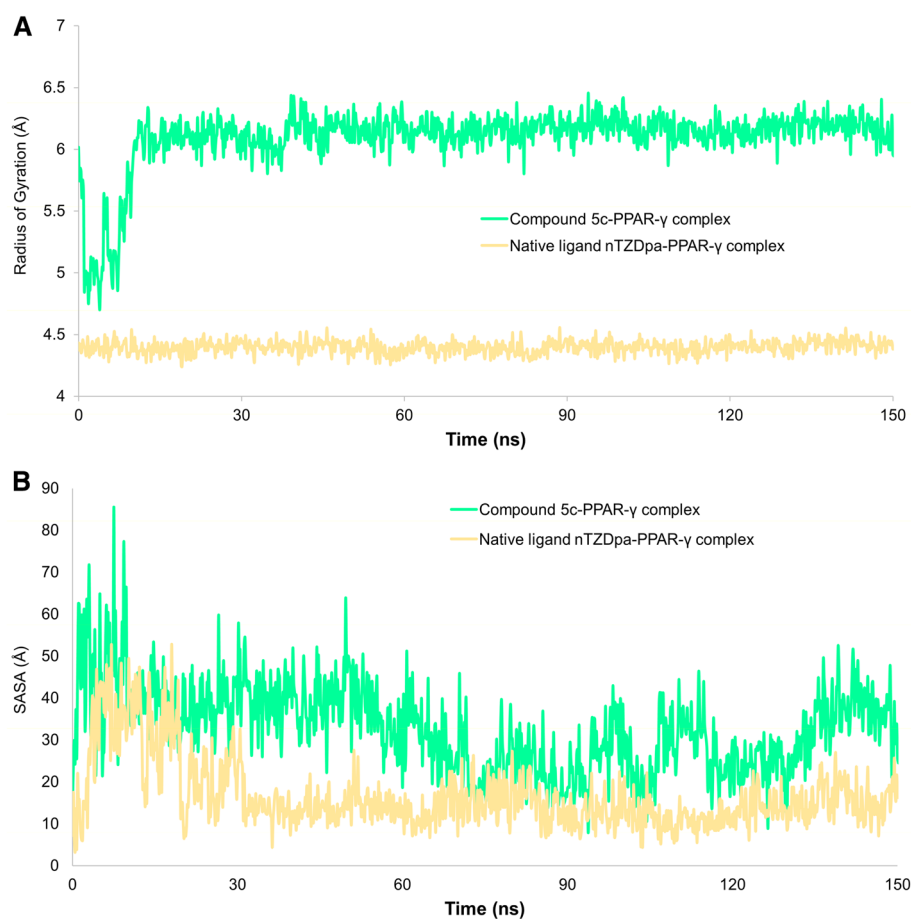


Figure 10. (A) Values of radius of gyration (rGyr); (B) solvent-accessible surface area (SASA) of the compounds 5c and nTZDpa bound to PPAR- γ protein during 150 ns MD simulation.

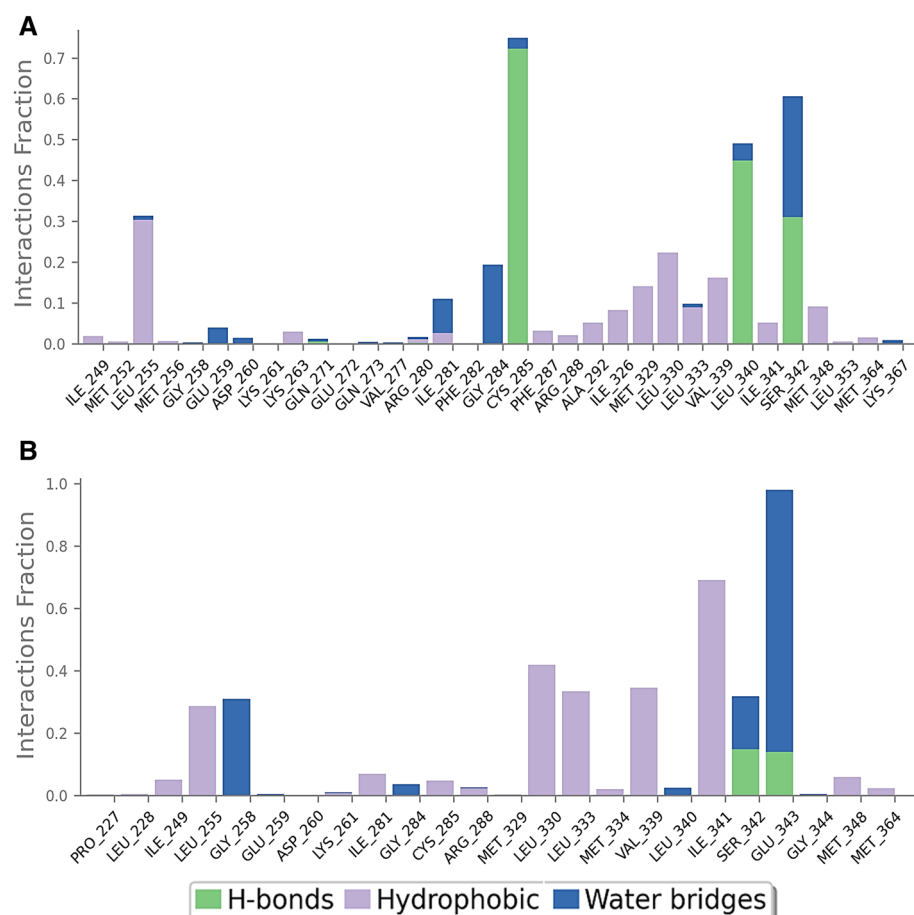


Figure 11. Intermolecular interactions of (A) compounds 5c; (B) nTZDpa with PPAR- γ , monitored throughout the simulation period of 150 ns. H-bonds, hydrophobic, and water bridge interactions are grouped by type and presented in a bar diagram.

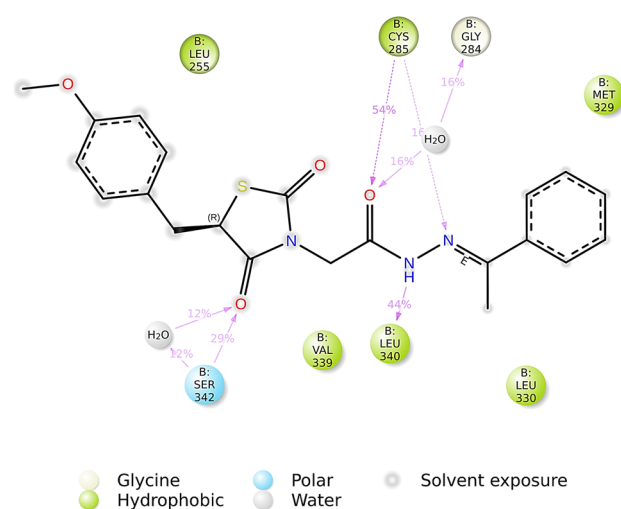


Figure 12. 2D depiction of nature and stability of binding interactions of compound 5c with PPAR- γ , observed throughout the MD simulation period of 150 ns.

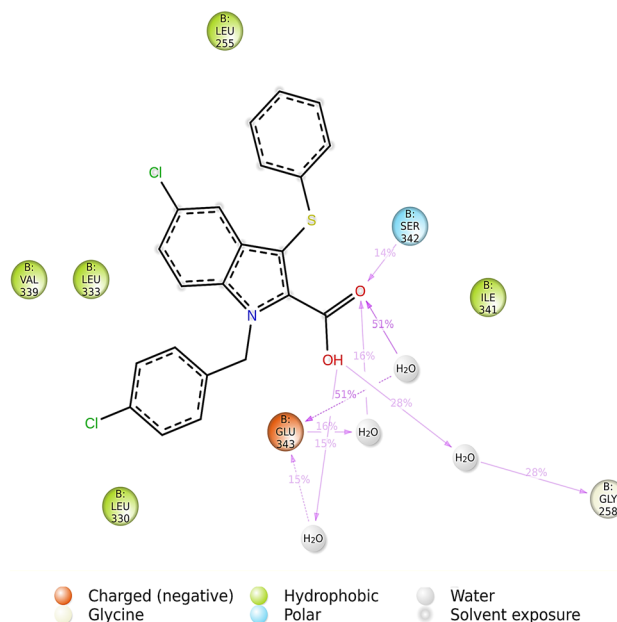


Figure 13. 2D depiction of nature and stability of binding interactions of nTZDpa with PPAR- γ , observed throughout the MD simulation period of 150 ns.

A deeper shade of orange indicates specific residues making more than one contact with the ligand. Fig. S2 is the timeline graph of nTZDpa presenting its various interactions with PPAR- γ . We have also supplied Video S3 which shows the movements of compound **5c** inside the binding site of PPAR- γ during MD simulation. In summary, MD simulations indicated that compound **5c** existed in a stable conformation inside the PPAR- γ binding site establishing stable hydrogen bonds with critical residues, confirming its potential to serve as partial agonist of PPAR- γ which requires further experimental validations.

Conclusions

The developed benzylidene 2,4-thiazolidinediones proved to be promising antidiabetic compounds that partially agonize the PPAR- γ receptors. The results of *in vivo* and *in silico* investigations were in agreement with those from the structure–activity relationship studies, leading to the identification of derivatives with comparable antidiabetic activity to the standard drug rosiglitazone. The molecular docking and molecular dynamics studies suggested that the title compounds bind to the same location as the native ligand, acting as a partial agonist at the receptor. The title compounds mainly interacted with the receptor via hydrophobic interactions; the introduction of a hydrogen bond acceptor, such as oxygen, to the compound resulted in hydrogen bonding and increased binding energy. All the required characteristic features of a partial agonist were present in the most active tested compounds, suggesting their partial PPAR- γ agonistic mechanism. Further specific *in vitro* and *ex vivo* molecular level studies are required to establish the exact mechanism. The most active compounds of this series can act as potential leads whose structure can be modified to further improve their efficacy.

Data availability

The datasets used and/or analyzed during the current study are available from the corresponding author upon reasonable request.

Received: 2 June 2023; Accepted: 9 November 2023

Published online: 14 November 2023

References

- Sun, H. *et al.* IDF Diabetes Atlas: Global, regional and country-level diabetes prevalence estimates for 2021 and projections for 2045. *Diabetes Res. Clin. Pract.* **183**, 109119. <https://doi.org/10.1016/j.diabres.2021.109119> (2022).
- Chaudhury, A. *et al.* Clinical review of antidiabetic drugs: Implications for type 2 diabetes mellitus management. *Front. Endocrinol. (Lausanne)* **8**, 6. <https://doi.org/10.3389/fendo.2017.00006> (2017).
- Padhi, S., Nayak, A. K. & Behera, A. Type II diabetes mellitus: A review on recent drug based therapeutics. *Biomed. Pharmacother.* **131**, 110708. <https://doi.org/10.1016/j.biopha.2020.110708> (2020).
- Ahsan, W. The journey of thiazolidinediones as modulators of PPARs for the management of diabetes: A current perspective. *Curr. Pharm. Des.* **25**(23), 2540–2554. <https://doi.org/10.2174/1381612825666190716094852> (2019).
- Ko, K. D., Kim, K. K. & Lee, K. R. Does weight gain associated with thiazolidinedione use negatively affect cardiometabolic health?. *J. Obes. Metab. Syndr.* **26**(2), 102–106. <https://doi.org/10.7570/jomes.2017.26.2.102> (2017).
- Corrales, P., Vidal-Puig, A. & Medina-Gómez, G. PPARs and metabolic disorders associated with challenged adipose tissue plasticity. *Int. J. Mol. Sci.* **19**(7), 2124. <https://doi.org/10.3390/ijms19072124> (2018).

7. Goltsman, I., Khoury, E. E., Winaver, J. & Abassi, Z. Does Thiazolidinedione therapy exacerbate fluid retention in congestive heart failure?. *Pharmacol. Ther.* **168**, 75–97. <https://doi.org/10.1016/j.pharmthera.2016.09.007> (2016).
8. Banerjee, S. *et al.* Type II diabetes mellitus and obesity: Common links, existing therapeutics and future developments. *J. Biosci.* **44**(6), 150 (2019).
9. Ballav, S., Biswas, B., Sahu, V. K., Ranjan, A. & Basu, S. PPAR- γ partial agonists in disease-fate decision with special reference to cancer. *Cells.* **11**(20), 3215. <https://doi.org/10.3390/cells11203215> (2022).
10. Thangavel, N., Al Bratty, M., Akhtar Javed, S., Ahsan, W. & Alhazmi, H. A. Targeting peroxisome proliferator-activated receptors using thiazolidinediones: Strategy for design of novel antidiabetic drugs. *Int. J. Med. Chem.* **2017**, 1069718. <https://doi.org/10.1155/2017/1069718> (2017).
11. Kroker, A. J. & Bruning, J. B. Review of the structural and dynamic mechanisms of PPAR γ partial agonism. *PPAR Res.* **2015**, 816856. <https://doi.org/10.1155/2015/816856> (2015).
12. Welday Kahssay, S., Hailu, G. S. & Taye, D. K. Design, synthesis, characterization and in vivo antidiabetic activity evaluation of some chalcone derivatives. *Drug Des. Dev. Ther.* **15**, 3119–3129. <https://doi.org/10.2147/DDDT.S316185> (2021).
13. OECD, *Test No. 425: Acute Oral Toxicity: Up-and-Down Procedure*, OECD Guidelines for the Testing of Chemicals, Section 4. (OECD Publishing, 2022). <https://doi.org/10.1787/9789264071049-en>.
14. Genuth, S.M., Palmer, J.P. & Nathan, D.M. Classification and diagnosis of diabetes. In *Diabetes in America* (Cowie, C.C., Casagrande, S.S., Menke, A., Cissell, M.A., Eberhardt, M.S., Meigs, J.B., Gregg, E.W., Knowler, W.C., Barrett-Connor, E., Becker, D.J., Brancati, F.L., Boyko, E.J., Herman, W.H., Howard, B.V., Narayan, K.M.V., Rewers, M. & Fradkin, J.E. eds.). 3rd Ed. Chap. 1. (National Institute of Diabetes and Digestive and Kidney Diseases (US), 2018).
15. Parsa, H., Moradi-Khaligh, Z., Rajabi, S., Ranjbar, K. & Komaki, A. Swimming training and Plantago psyllium ameliorate cognitive impairment and glucose tolerance in streptozotocin-nicotinamide-induced type 2 diabetic rats. *J. Physiol. Sci.* **71**(1), 37. <https://doi.org/10.1186/s12576-021-00823-z> (2021) (**erratum in: J Physiol Sci.** **2022**;72(1):20).
16. Oliyaei, N., Moosavi-Nasab, M., Tamaddon, A. M. & Tanideh, N. Antidiabetic effect of fucoxanthin extracted from Sargassum-gustifolium on streptozotocin-nicotinamide-induced type 2 diabetic mice. *Food Sci. Nutr.* **9**(7), 3521–3529. <https://doi.org/10.1002/fsn3.2301> (2021).
17. Zhang, S. *et al.* Structure-based drug design of an inhibitor of the SARS-CoV-2 (COVID-19) main protease using free software: A tutorial for students and scientists. *Eur. J. Med. Chem.* **218**, 113390. <https://doi.org/10.1016/j.ejmech.2021.113390> (2021).
18. Kohlbacher, S. M., Langer, T. & Seidel, T. QPHAR: Quantitative pharmacophore activity relationship: Method and validation. *J. Cheminform.* **13**, 57. <https://doi.org/10.1186/s13321-021-00537-9> (2021).
19. Thangavel, N. & Albratty, M. Pharmacophore model-aided virtual screening combined with comparative molecular docking and molecular dynamics for identification of marine natural products as SARS-CoV-2 papain-like protease inhibitors. *Arab. J. Chem.* **15**(12), 104334. <https://doi.org/10.1016/j.arabjc.2022.104334> (2022).
20. Miyamae, Y. Insights into dynamic mechanism of ligand binding to peroxisome proliferator-activated receptor γ toward potential pharmacological applications. *Biol. Pharm. Bull.* **44**(9), 1185–1195. <https://doi.org/10.1248/bpb.b21-00263> (2021).
21. Capelli, D. *et al.* Structural basis for PPAR partial or full activation revealed by a novel ligand binding mode. *Sci. Rep.* **6**, 34792. <https://doi.org/10.1038/srep34792> (2016).
22. Bruning, J. B. *et al.* Partial agonists activate PPAR γ using a helix 12 independent mechanism. *Structure.* **15**(10), 1258–1271. <https://doi.org/10.1016/j.str.2007.07.014> (2007).
23. Hughes, T. S. *et al.* An alternate binding site for PPAR γ ligands. *Nat. Commun.* **5**, 3571. <https://doi.org/10.1038/ncomms4571> (2014).
24. Hou, Y. *et al.* CMHX008, a PPAR γ partial agonist, enhances insulin sensitivity with minor influences on bone loss. *Genes Dis.* **5**(3), 290–299. <https://doi.org/10.1016/j.gendis.2018.05.004> (2018).
25. Giordano, D., Biancaniello, C., Argenio, M. A. & Facchiano, A. Drug design by pharmacophore and virtual screening approach. *Pharmaceuticals.* **15**(5), 646. <https://doi.org/10.3390/ph15050646> (2022).

Acknowledgements

The authors extend their appreciation to the Deanship of Scientific Research, Jazan University, Jazan Saudi Arabia for funding this Research work through the Waed project number W41-035.

Author contributions

A.N., M.A. and H.A.A. conceptualized the study, did general supervision and project administration; A.N. and M.S.A. performed synthesis and purification of compounds and assisted in writing the manuscript; N.T. performed molecular docking study and assisted in writing the manuscript; F.A. performed MD simulation studies and helped in revising the manuscript; M.M.E.T. performed animal studies and assisted in writing the manuscript; A.M.M. performed statistical analysis and assisted in writing the manuscript; W.A. wrote and revised the manuscript; A.H. performed characterization of synthesized compounds.

Funding

This work was funded by the Deanship of Scientific Research, Jazan University, Jazan Saudi Arabia through the Waed project with number W41-035.

Competing interests

The authors declare no competing interests.

Additional information

Supplementary Information The online version contains supplementary material available at <https://doi.org/10.1038/s41598-023-47157-x>.

Correspondence and requests for materials should be addressed to A.N.

Reprints and permissions information is available at www.nature.com/reprints.

Publisher's note Springer Nature remains neutral with regard to jurisdictional claims in published maps and institutional affiliations.



Open Access This article is licensed under a Creative Commons Attribution 4.0 International License, which permits use, sharing, adaptation, distribution and reproduction in any medium or format, as long as you give appropriate credit to the original author(s) and the source, provide a link to the Creative Commons licence, and indicate if changes were made. The images or other third party material in this article are included in the article's Creative Commons licence, unless indicated otherwise in a credit line to the material. If material is not included in the article's Creative Commons licence and your intended use is not permitted by statutory regulation or exceeds the permitted use, you will need to obtain permission directly from the copyright holder. To view a copy of this licence, visit <http://creativecommons.org/licenses/by/4.0/>.

© The Author(s) 2023